IEEE Access
Multidisciplinary ⋮ Rapid Review ⋮ Open Access Journal

Date of publication xxxx 00, 20xx, date of current version July 7, 2019.

Digital Object Identifier xxxxyyyyzzzz

Noncoherent detection for ambient backscatter communications over OFDM signals

DONATELLA DARSENA[1], (Senior Member, IEEE)
[1]Department of Engineering, Parthenope University, Naples I-80143, Italy (e-mail: darsena@uniparthenope.it)
Corresponding author: Donatella Darsena (e-mail: darsena@uniparthenope.it).

ABSTRACT

Backscattering communications have been recently proposed as an effective enabling technology for massive Internet of Things (IoT) development. A novel application of backscattering, called ambient backscattering (AmBC), has been gaining much attention, wherein backscattering communications exploit existing RF signals without the need for a dedicated transmitter. In such a system, data demodulation process is strongly complicated by the random nature of the illuminating signal, as well as by the presence of the direct-link interference (DLI) from the legacy system. To overcome these shortcomings, one can resort to noncoherent detection strategies, aimed at reducing or even nullifying the amount of *a priori* information needed to reliably perform signal demodulation. In this paper, we investigate noncoherent detection strategies for backscatter communications over ambient OFDM signals and solve the noncoherent maximum-likelihood (ML) detection problem for a general Q-ary signal constellation. Additionally, we derive a suboptimal detector, which takes the form of the classical energy-detector (ED), whose performance is evaluated in closed-form. Finally, the performance of the proposed detectors is corroborated through Monte Carlo simulations.

INDEX TERMS Ambient backscatter, noncoherent detection, maximum-likelihood criterion, energy-detector, performance analysis.

I. INTRODUCTION

WITH the advent of Internet of Things (IoT) [1], [2], where Internet extends into the real world [3] and billions of devices sense the surrounding environment and communicate without human intervention, a key issue is the search for energy-efficient reliable sensing communication protocols, which can support large-scale and seamless deployment by relaxing battery constraints. For this reason, *backscattering communications* [4]–[8] have been recently proposed as an effective enabling technology for massive IoT development.

Backscattering refers to the process where a device transmits its information by reflecting and modulating an illuminating RF signal, without employing an active RF transceiver. A well-known application of backscattering communications is the RFID technology [9], [10], where an active device, called reader, transmits an unmodulated RF signal towards a certain number of passive tags, which reply by backscattering the signal to transmit their data to the reader. Recently, a novel application of backscattering, called *ambient backscattering* (AmBC), has been gaining much attention [11], [12], wherein backscattering communication exploits existing or *legacy* RF signals (such as digital television, cellular, wireless LAN, or Wi-Fi systems), without the need for a dedicated transmitter. Differently from traditional RFID technology, AmBC systems enable [11] device-to-device communication and, furthermore, reduce EM pollution by opportunistically leveraging on existing RF signals.

Although AmBC technology might have a significant impact on enabling low-power ubiquitous IoT, its diffusion is still limited due to several problems that need to be addressed. In particular, data demodulation at the AmBC reader represents a challenging task, for two reasons. First, the reader receives the weak backscattered signal together with the unknown stronger direct-link interference (DLI) generated by the RF legacy source. Second, different from a conventional RFID system, the illuminating signal is an unknown (random) modulated signal, which complicates

backscatter signal detection.

DLI suppression in AmBC system is much more complicated than in RFID systems, where the DLI is an unmodulated signal that is generated by the reader itself whose effects can be mitigated by resorting to analog and/or digital self-interference suppression techniques [13]. Some recent studies focus on the employment of multiple antennas at the reader to improve the backscatter performance in highly DLI-contaminated AmBC environments [14]–[18]. In [19], the authors propose to employ two antennas at the tag, with different transmit power levels, while in [20] a statistical covariance-based signal detection technique is considered, whose implementation requires the availability of large amount of samples.

Other studies assume that the legacy system employs Orthogonal Frequency Division Multiplexing (OFDM) and mitigates the DLI by exploiting some structural properties of the modulation format. In [21], the DLI is canceled out by exploiting the *unconsumed* part of the cyclic prefix (CP) of the OFDM symbols; the proposed receiver does not require knowledge of the legacy RF signal, but requires estimation of the strength of the backscatter channel and fails if the channel delay spread is equal to the CP length (i.e., the unconsumed part of CP is null). The authors in [22], instead, design the tag modulation waveform so as to shift the backscattered energy in correspondence of the null subcarriers of the ambient OFDM signal and use an energy detector to blindly (i.e., without requiring knowledge of the ambient signal and/or the channels) decode the tag information. This approach, however, requires a more complicated operation carried out by the tag which, moreover, must know in advance the number and positions of the null subcarrier in the legacy OFDM signal. A cloud radio access network (C-RAN) architecture has been recently proposed in [23] to jointly cope with DLI suppression and imperfect channel estimation, which, however, requires a high-speed wired fronthaul link to a centralized cloud processor.

Due to the lack of knowledge of the RF legacy signal, the adoption of coherent detection at the reader requires a pilot-assisted channel estimation phase and a strong coordination between the legacy and the backscatter systems. A viable alternative is the use of *semi-coherent* or *noncoherent* detection strategies, aimed at reducing or even nullifying the amount of *a priori* information needed to reliably perform signal detection. In [24], modeling the ambient RF signals as circularly symmetric complex Gaussian random processes, a maximum-likelihood (ML) semicoherent detector for a frequency-flat channel model is proposed, which, however, requires some form of channel estimation. In [25], instead, a ternary-symbol-based coding scheme is devised, which, coupled with a maximum a posteriori probability detector, assures a throughput increase, but still relies on the knowledge/estimation of the composite channels at the reader. A noncoherent detection strategy for bistatic scatter radio is devised in [8]. Increasing the complexity of the tag, use of differential coding has been considered for AmBC systems

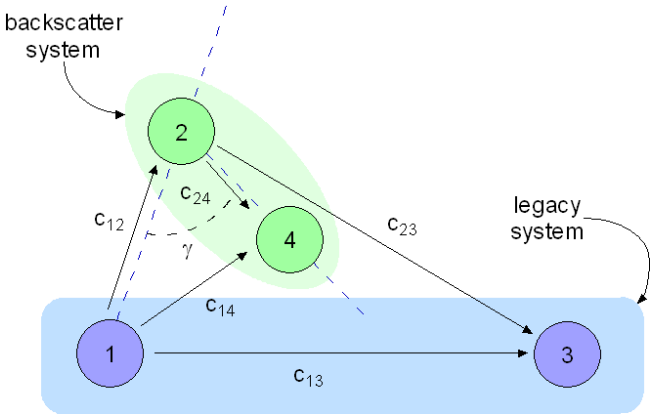

Figure 1: Ambient backscatter system consisting of a legacy system (nodes 1 and 3), a tag (node 2) and a reader (node 4).

in [26], [27], and semi-coherent and noncoherent detection approaches are examined. At high SNR and for large data samples available at the reader, a noncoherent detector is proposed in [28].

In this paper, we investigate noncoherent detection problem for backscatter communications over ambient OFDM signals. The main contributions of the paper can be summarized as follows:

- We formulate and solve the noncoherent ML detection problem for a general Q-ary backscatter signal over ambient OFDM modulation, by treating the DLI as an unwanted signal, modeled as a random process that is correlated, through legacy symbols, to the useful backscatter signal contribution.
- Relying on a minimal set of assumptions, a ML detector is derived, which does not require *a priori* knowledge about the instantaneous channels or legacy symbols and does not entail complicated operations carried out by the tag.
- We particularize our detector to the case of on-off keying (OOK) backscatter signaling and equal-energy legacy symbols, by expressing the threshold detector in closed-form.
- We derive a *suboptimal* detector, which takes the form of the classical energy-detector (ED), whose performance is evaluated in closed-form.

Moreover, we provide numerical results aimed at corroborating our design and study the effect of different parameters on the performance of the proposed detectors, such as the number of OFDM subcarriers, the signal-to-noise ratio (SNR) and the signal-to-interference ratio (SIR), i.e., the ratio between the power of the backscatter signal and DLI.

The rest of the paper is organized as follows. In Section II, we present the system model. In Section III, the noncoherent ML detection problem is addressed. In Section IV, we derive the suboptimal energy detector. In Section V, numerical results are reported and, finally, Section VI draws conclusions.

II. SYSTEM MODEL

As depicted in Fig. 1, we consider a wireless network composed by a legacy[1] system, encompassing a transmitter-receiver pair (node 1 and 3), and an AmBC system, composed by a single-antenna tag (node 2) and a single-antenna reader (node 4). The tag is a passive device, i.e., it does not include any active RF component, and uses the energy harvested from the ambient RF signal to power up its circuit and perform data communications by backscattering.

The legacy system employs OFDM with M subcarriers, cyclic prefix (CP) of length $L_{\rm cp} < M$, and symbol period T, whose symbols $s[n]$ are modeled as random variables having variance $\sigma_s^2 \triangleq \mathsf{E}[|s[n]|^2]$. At the OFDM transmitter, the symbol vector $\boldsymbol{s}[n] \triangleq [s[nM], s[nM+1], \ldots, s[nM+M-1]]^{\rm T}$ undergoes standard OFDM precoding, encompassing inverse discrete Fourier transform (IDFT) and CP insertion; after parallel-to-serial (P/S) conversion, it feeds a digital-to-analog converter (DAC) operating at rate $f_s \triangleq 1/T_s = P/T$, where T_s is the sampling period and $P \triangleq M + L_{\rm cp}$. Before being transmitted over the wireless channel, the continuous-time signal $u(t)$ generated by the DAC is up-converted, giving thus $\widetilde{u}(t) \triangleq \mathrm{Re}\{u(t)\, e^{j2\pi f_c t}\}$, where $\widetilde{u}(t)$ is the continuous-time bandpass transmitted OFDM signal and f_c represents the carrier frequency of the OFDM source.

From Fig. 1, the bandpass OFDM signal received at the tag can be expressed as

$$\widetilde{z}(t) = \mathrm{Re}\{[u(t-d_{12}) * c_{12}(t)]\, e^{j2\pi f_c (t-d_{12})}\} \qquad (1)$$

where $c_{ik}(t)$ denotes the baseband channel impulse response (CIR) between nodes i and k, for $(i,k) \in \{(1,2),(2,4),(1,4)\}$, with multipath delay spread τ_{ik} and link propagation delay d_{ik}. Observe that, since the tag usually contains only passive electronic components and performs low-power analog operations, the thermal noise at the tag is neglected [21], [22].

Let us denote with $\{b[\ell]\}_{\ell\in\mathbb{Z}}$ the information symbols that the tag wishes to transmit towards the reader (node 4), modeled as a sequence of i.i.d. random variables, with variance $\sigma_b^2 \triangleq \mathsf{E}[|b[\ell]|^2]$. Due to power limitations, the tag usually transmits at much lower rates than $1/T_s$; in particular, we will assume in the sequel that the tag transmission rate is equal to $1/T$, i.e., only one symbol $b[\ell]$ is transmitted for each OFDM block. Let $b(t)$ be the continuous-time baseband signal transmitted by the tag; focusing, without loss of generality, on the n-th OFDM symbol period, the signal backscattered by the tag is given by

$$\widetilde{y}(t) \triangleq \alpha\, b(nT)\, \widetilde{z}(t)\,, \quad \text{for } t \in [nT, (n+1)T] \qquad (2)$$

where $0 \le \alpha \le 1$ is a scaling factor, which takes into account the scattering efficiency and the antenna gain of the tag in the transmitting direction [5]. Timing acquisition can be performed by both tag and reader by exploiting the repetitive structure in the time domain of the legacy signal [31]. A timing estimator can be designed, for example, by searching for the peak of the correlation among repetitive parts of the OFDM signal, without requiring the knowledge of the ambient signal [21]; in the following, we will assume that time synchronization has been acquired by both tag and reader.

On the basis of (1) and (2), after down-conversion and assuming the multipath channel spread of the link $1 \to 2 \to 4$ much smaller than the symbol period T, it turns out that the baseband signal received at the reader[2] (node 4) can be expressed as [23]

$$\begin{aligned} r(t) &= \alpha\, b(nT)\, [z(t-d_{24}) * c_{24}(t)] \\ &\quad + u(t-d_{14}) * c_{14}(t) + w(t) \\ &= \alpha\, b(nT)\, [u(t-d_{12}-d_{24}) * c_{12}(t-d_{24}) * c_{24}(t)] \\ &\quad + u(t-d_{14}) * c_{14}(t) + w(t) \\ &= r_{\rm BS}(t) + r_{\rm DLI}(t) + w(t) \end{aligned} \qquad (3)$$

for $t \in [nT, (n+1)T]$, where $r_{\rm BS}(t) \triangleq \alpha\, b(nT)\, [u(t-d_{12}-d_{24}) * c_{12}(t-d_{24}) * c_{24}(t)]$ is the backscattered signal at the receiver, which contains the backscatter information symbols $b[\ell]$ to be detected, $r_{\rm DLI}(t) \triangleq u(t-d_{14}) * c_{14}(t)$ represents the direct-link (i.e., link $1 \to 4$) interference from the OFDM source, whereas $w(t)$ is the additive noise, assumed to be statistically independent of $r_{\rm BS}(t)$ and $r_{\rm DLI}(t)$.

Usually, the scaling factor[3] α assumes small values and, thus, the energy reflected towards the backscatter receiver is less than that is harvested and/or dissipated by the tag, due to antenna and modulator losses. Hence, the backscattered signal $r_{\rm BS}(t)$ may be much weaker than the direct-link interference $r_{\rm DLI}(t)$, also because, differently from $r_{\rm DLI}(t)$, it suffers from round-trip channel attenuation, i.e., the links $1 \to 2$ and $2 \to 4$, making backscatter signal detection a very challenging task.

Turning to the discrete-time signal model, let us define $D_{ik} \triangleq \lfloor d_{ik}/T_s \rfloor$ and $\delta_{ik} \triangleq d_{ik} - D_{ik}\, T_s$ as the integer and the fractional part of the discrete-time propagation delay, respectively, of the link $i \to k$, for $(i,k) \in \{(1,2),(2,4),(1,4)\}$. Moreover, let $L_{ik} \triangleq \lfloor \tau_{ik}\, f_s \rfloor$ denote the channel memory and $c_{ik}[n] \triangleq c_{ik}(n\, T_s + \delta_{ik})$, the received signal (3) is sampled with rate $f_s = 1/T_s$ at time epochs $t_n \triangleq n\, T_s$, with $n \in \mathbb{Z}$, yielding thus the sequence[4]

[1] As in [11], the term *legacy* refers to existing wireless systems, such as, e.g., DTV, cellular, W-LAN, or Wi-Fi systems. Details regarding the medium access control (MAC) of the legacy system [29], [30] are omitted, since they are irrelevant for the proposed detection structures.

[2] We suppose that a possible carrier frequency offset (CFO) has been properly estimated and, subsequently, compensated [5].

[3] Note that we are assuming a simplified harvesting model, neglecting the possible nonlinear behavior of the energy harvesting circuit [32].

[4] Equation (4) rigorously holds for bandlimited signals [33] and represents a very good approximation in practice.

[21], [22]

$$\begin{aligned} r[n] &= \alpha\, b[nP]\,(u[n-D_{12}-D_{24}] * c_{12}[n-D_{24}] * c_{24}[n]) \\ &\quad + u[n-D_{14}] * c_{14}[n] + w[n] \\ &= \alpha\, b[nP] \sum_{k=0}^{L_{\rm c}} c_{124}[k]\, u[n-D_{\rm c}-k] \\ &\quad + \sum_{k=0}^{L_{14}} c_{14}[k]\, u[n-D_{14}-k] + w[n] \end{aligned} \tag{4}$$

where $c_{124}[n] \triangleq c_{12}[n] * c_{24}[n]$ represents the *composite* discrete-time channel of the link $1 \to 2 \to 4$, modeled as a causal FIR filter of order $L_{\rm c} \triangleq L_{12}+L_{24}$, $D_{\rm c} \triangleq D_{12}+2\,D_{24}$, and we set, for notation simplicity, $x[n] \triangleq x(nT_s)$. The discrete-time additive noise $w[n]$ is modeled as a sequence of i.i.d. circularly-symmetric complex Gaussian[5] random variables, with variance $\mathsf{E}[|w(n)|^2] \triangleq \sigma_w^2$.

The received stream $r[n]$ first undergoes serial-to-parallel (S/P) conversion and, then, is subject to CP removal and M-point discrete Fourier transform (DFT), yielding thus [35]

$$\boldsymbol{r}[m] \triangleq \alpha\, \boldsymbol{C}_{12}\, \boldsymbol{C}_{24}\, \boldsymbol{s}[m]\, b[m] + \boldsymbol{C}_{14}\, \boldsymbol{s}[m] + \boldsymbol{w}[m] \tag{5}$$

where the entries of the diagonal matrices $\boldsymbol{C}_{ik} \triangleq \mathrm{diag}[C_{ik}(0), C_{ik}(1), \ldots, C_{ik}(M-1)]$ are defined as

$$C_{ik}(q) \triangleq e^{-j\frac{2\pi}{M}D_{ik}q} \sum_{\ell=0}^{L_{ik}} c_{ik}(\ell)\, e^{-j\frac{2\pi}{M}\ell q} \tag{6}$$

for $(i,k) \in \{(1,2),(2,4),(1,4)\}$. It is worth noting that, provided that the CP length is greater than the maximum channel spread of the backscatter system, i.e., $L_{\rm cp} \geq L_{\max} \triangleq \max\{L_{\rm c}+D_{\rm c}, L_{14}+D_{14}\}$, CP removal guarantees perfect ISI suppression [35]. Due to the short distance among the OFDM source (node 1), the tag (node 2) and the reader (node 4), one can assume that the channel spread of the backscatter channel $(L_{\rm c}+D_{\rm c})T_s$ and that of the direct link $(L_{14}+D_{14})T_s$ are much lower than the legacy OFDM channel spread, and, consequently, the requirement $L_{\rm cp} \geq L_{\max}$ is not very restrictive in practice.

In the following, we assume fading Rayleigh channels by modeling the time-domain channel taps $\{c_{ik}(\ell)\}_{\ell=0}^{L_{ik}}$ as statistically independent circularly-symmetric complex Gaussian random variables [21], with variances $\mathsf{E}[|c_{ik}(\ell)|^2] \triangleq \sigma_{ik}^2/(L_{ik}+1)$, for any $\ell = 0, 1, \ldots, L_{ik}$. From (6) we note that the DFT samples $C_{ik}(q_1)$ and $C_{ik}(q_2)$ are correlated [23], for $q_1 \neq q_2$, i.e.,

$$\mathsf{E}[C_{ik}(q_1)\, C_{ik}^*(q_2)] = \frac{\sigma_{ik}^2}{L_{ik}+1} e^{-j\frac{2\pi}{M}\theta_{ik}(q_1-q_2)} \mathsf{D}_{L_{ik}+1}\left(\frac{q_1-q_2}{M}\right) \tag{7}$$

where, for $x \in \mathbb{R}$, we have defined the Dirichlet function

$$\mathsf{D}_N(x) \triangleq \frac{\sin(\pi N x)}{\sin(\pi x)}\, e^{-j\pi(N-1)x}\,.$$

[5]Note that, in some wireless scenarios, the noise may be non-Gaussian, but the proposed detectors can be suitably modified to account for the non-Gaussian nature of noise [34].

We note that, for $q_1, q_2 \in \{0, 1, \ldots, M-1\}$, with $q_1 \neq q_2$, it results

$$|\mathsf{E}[C_{ik}(q_1)\, C_{ik}^*(q_2)]| \leq \mathsf{E}[|C_{ik}(q_1)|^2] = \sigma_{ik}^2\,.$$

Obtaining a manageable closed-form expression for the noncoherent detector by taking into account the correlation among the OFDM subchannels is mathematically intractable. To simplify the problem, we will neglect the correlation among the subchannels [36], and model $C_{ik}(q)$, for $(i,k) \in \{(1,2),(2,4),(1,4)\}$ and any $q = 0, 1, \ldots, M-1$, as i.i.d. circularly-symmetric complex Gaussian random variables, with zero-mean and variances $\mathsf{E}[|C_{ik}(q)|^2] = \sigma_{ik}^2$.

Relying on (5), the SIR can be defined as

$$\begin{aligned} \mathrm{SIR} &\triangleq \frac{\mathsf{E}[\|\alpha\, \boldsymbol{C}_{12}\, \boldsymbol{C}_{24}\, \boldsymbol{s}[m]\, b[m]\|^2]}{\mathsf{E}[\|\boldsymbol{C}_{14}\, \boldsymbol{s}[m]\|^2]} && (8) \\ &= \alpha^2\, \frac{\mathrm{trace}\{\mathsf{E}[|b[m]|^2\, \boldsymbol{C}_{12}\, \boldsymbol{C}_{24} \boldsymbol{s}[m]\, \boldsymbol{s}^{\rm H}[m]\, \boldsymbol{C}_{24}^*\, \boldsymbol{C}_{12}^*]\}}{\mathrm{trace}\{\mathsf{E}[\boldsymbol{C}_{14}\, \boldsymbol{s}[m]\, \boldsymbol{s}^{\rm H}[m]\, \boldsymbol{C}_{14}^*]\}} \\ &= \alpha^2\, \sigma_b^2\, \frac{\mathrm{trace}\{\mathsf{E}[|\boldsymbol{C}_{12}|^2] \cdot \mathsf{E}[|\boldsymbol{C}_{24}|^2]\}}{\mathrm{trace}\{\mathsf{E}[|\boldsymbol{C}_{14}|^2]\}} && (9) \\ &= \alpha^2\, \sigma_b^2\, \frac{\sigma_{12}^2\, \sigma_{24}^2}{\sigma_{14}^2} && (10) \end{aligned}$$

where we have exploited the statistical independence among the involved variables.

As regards the legacy system, it is worthwhile to note that the backscattered signal (2) is also received by the legacy OFDM receiver (node 3), resulting in a weak interference contribution, which affects the direct OFDM signal propagated through the link $1 \to 3$. More precisely, the signal backscattered by the tag may create additional paths on the link $1 \to 3$, increasing the corresponding multipath delay spread and possibly causing a performance degradation of the legacy OFDM system, due to the presence of ISI after CP removal. However, as shown in [35], if the CP duration spans more than the maximum delay spread between the direct channel (i.e., $1 \to 3$) and the composite channel (i.e., $1 \to 2 \to 3$), the legacy system might *even* achieve a small performance gain. In [35] it is proven, indeed, that the presence of AmBC can increase the ergodic capacity of the legacy system, since the interference generated by the backscatter communication results in a form of diversity for the legacy system.

III. NONCOHERENT MAXIMUM-LIKELIHOOD DEMODULATION

In this section, we address the problem of noncoherent ML demodulation of AmBC signals. The strict constraints in terms of available energy, memory and computational complexity strongly limit the length of the transmitted backscatter packets, complicating, in practice, training-based [23] channel estimation required for coherent detection of the backscatter symbols $b[m]$ at the reader. On the other hand, the reader does not usually have *a priori* information about the legacy transmission, which is also required to perform coherent detection, motivating the need to study noncoherent

detection structures. To design a demodulator that operates without the assumption that the legacy symbols $\boldsymbol{s}[m]$ and the channels $\boldsymbol{C}_{ik}$ for $(i,k) \in \{(12),(2,4),(1,4)\}$ are known at the node 4, we first evaluate the ML function of the transmitted backscatter signals conditioned on the value of $\boldsymbol{s}[m]$ and $\boldsymbol{C}_{ik}$ and, then, average over them [37].

In the following, we assume that backscatter modulation is memoryless, whose symbols $b[m]$ are independently and equiprobably drawn from a finite-size set $B \triangleq \{\beta_0, \beta_1, \ldots, \beta_{Q-1}\}$. Without loss of generality, we restrict our attention to the time interval $[0, T]$ and, for simplicity of notation, we omit hereinafter the temporal variable m. The detector has to decide among the Q hyphotheses

$$H_q: \quad \boldsymbol{r} = \alpha\, \boldsymbol{C}_{12}\, \boldsymbol{C}_{24}\, \boldsymbol{s}\, \beta_q + \boldsymbol{C}_{14}\, \boldsymbol{s} + \boldsymbol{w} \quad q = 0, 1, \ldots, Q-1$$

on the basis of the observation of $\boldsymbol{r}$; the adopted decision rule is

$$\hat{b} \triangleq \arg \max_{\beta_q \in B} \mathsf{E}_{\boldsymbol{C}_{12}, \boldsymbol{C}_{24}, \boldsymbol{C}_{14}, \boldsymbol{s}} \left[f_{\boldsymbol{r}|\boldsymbol{C}_{12}, \boldsymbol{C}_{24}, \boldsymbol{C}_{14}, \boldsymbol{s}}(\boldsymbol{r}; \beta_q) \right] \tag{11}$$

where $f_{\boldsymbol{r}|\boldsymbol{C}_{12}, \boldsymbol{C}_{24}, \boldsymbol{C}_{14}, \boldsymbol{s}}(\boldsymbol{r}; \beta_q)$ is the multivariate probability density function (pdf) of the received vector $\boldsymbol{r}$, under the q-th hyphotesis H_q, conditioned on $\boldsymbol{C}_{12}$, $\boldsymbol{C}_{24}$, $\boldsymbol{C}_{14}$, and $\boldsymbol{s}$. By invoking the conditional expectation rule [38] and the statistical independence among $\boldsymbol{C}_{12}$, $\boldsymbol{C}_{24}$, $\boldsymbol{C}_{14}$, and $\boldsymbol{s}$, the decision rule (11) can be rewritten as

$$\hat{b} \triangleq \arg \max_{\beta_q \in B} \mathsf{E}_{\boldsymbol{s}}[\mathsf{E}_{\boldsymbol{C}_{24}}[\mathsf{E}_{\boldsymbol{C}_{14}}[\mathsf{E}_{\boldsymbol{C}_{12}}[f_{\boldsymbol{r}|\boldsymbol{C}_{12}, \boldsymbol{C}_{24}, \boldsymbol{C}_{14}, \boldsymbol{s}}(\boldsymbol{r}; \beta_q)]]]] \,. \tag{12}$$

Lemma 1: The noncoherent detector expressed by (12) is equivalent to

$$\hat{b} \triangleq \arg \max_{\beta_q \in B} \mathsf{E}_{\boldsymbol{s}} \left[\prod_{k=0}^{M-1} g_{kq}\left(|r_k|^2; \beta_q\right) \right] \tag{13}$$

where

$$g_{kq}(|r_k|^2; \beta_q) \triangleq \begin{cases} \frac{\sigma_w^2}{\sigma_{24}^2 \gamma_{kq}} \exp\left(\frac{\delta_k}{\sigma_{24}^2 \gamma_{kq}}\right) K_0\left(\frac{|r_k|^2}{\delta_k}, \frac{\delta_k}{\sigma_{24}^2 \gamma_{kq}}\right), & \text{for } \gamma_{kq} \neq 0; \\ \frac{\sigma_w^2}{\delta_k} \exp\left(-\frac{|r_k|^2}{\delta_k}\right), & \text{for } \gamma_{kq} = 0 \end{cases} \tag{14}$$

with $\gamma_{kq} \triangleq \alpha^2\, \sigma_{12}^2\, |\beta_q|^2\, |s_k|^2$, $\delta_k \triangleq \sigma_w^2 + \sigma_{14}^2\, |s_k|^2$, and

$$K_0(x, y) = \int_1^{+\infty} t^{-1}\, \mathrm{e}^{-x\, t - y\, t^{-1}}\, \mathrm{d}t$$

denoting the *leaky aquifer function* [39].

Proof: See Appendix . ∎

We observe that the noncoherent detector depends on the squared values of the received symbols r_k, for $k = 0, 1, \ldots, M-1$, as expected.

Remark 1: When constant-modulus legacy symbols are transmitted, the terms $|s_k|^2$ are all equal and, thus, the statistical average with respect to $\boldsymbol{s}$ in (13) can be discarded.

Remark 2: From (13), it is apparent that the backscatter system can employ only non constant-modulus constellations, for which $|\beta_i| \neq |\beta_k|$ with $i \neq k$. It is well-known [40] that the average energy $\mathcal{E} = \frac{1}{Q} \sum_{i=1}^{Q} |a_i|^2$ required for transmission of a constellation with equiprobable points $\{a_i\}_{i=1}^{Q}$ is minimized if $\sum_{i=1}^{Q} a_i = 0$, i.e., if its center of gravity is at the origin. Since non constant-modulus constellations employed for noncoherent detection do not satisfy this condition, they require, for a given error probability, an expenditure of energy higher than that of their constant-modulus counterparts [40].

Remark 3: The function

$$K_\nu(x, y) = \int_1^{+\infty} t^{-\nu-1}\, \mathrm{e}^{-x\, t - y\, t^{-1}}\, \mathrm{d}t$$

is related to the modified Bessel function

$$K_\nu(z) = \frac{1}{2} \int_0^{+\infty} t^{-\nu-1}\, \mathrm{e}^{-z(t + t^{-1})}\, \mathrm{d}t \,.$$

For $\nu = 0$, it is known as *leaky aquifer function*, because it is used to describe water levels in pumped aquifer systems with finite transmissivity [39]. Closed forms of this function, in terms of modified Bessel functions and error functions, exist only for $\nu = 1/2 - n$, with $n \in \mathbb{N} \cup \{0\}$. However, by using expansions of this function that are designed for specific parameter ranges, the leaky aquifer function can be computed very efficiently [41]. Moreover, also in its integral form, it can be easily and efficiently implemented through standard quadrature routines [39], provided by common software packages (e.g., Matlab, Mathematica).

A special case occurs when equal-energy legacy symbols are transmitted and the tag employs equiprobable OOK signaling (on-off), for which $\sigma_b^2 = 1/2$. In this case, the decision rule (13) reduces to

$$\prod_{k=0}^{M-1} \frac{\sigma_w^2}{\sigma_{24}^2\, \gamma} \exp\left(\frac{\delta}{\sigma_{24}^2\, \gamma}\right) K_0\left(\frac{|r_k|^2}{\delta}, \frac{\delta}{\sigma_{24}^2\, \gamma}\right) \underset{0}{\overset{1}{\gtrless}} \prod_{k=0}^{M-1} \frac{\sigma_w^2}{\delta} \exp\left(-\frac{|r_k|^2}{\delta}\right) \tag{15}$$

where $\gamma = \alpha^2\, \sigma_{12}^2\, \sigma_s^2$ and $\delta = \sigma_w^2 + \sigma_{14}^2\, \sigma_s^2$ become independent of the subcarrier index k. Through a few simple manipulations, taking the logarithm of both sides of equation (15) yields

$$\frac{1}{\delta} \|\boldsymbol{r}\|^2 + \sum_{k=0}^{M-1} \log\left[K_0\left(\frac{|r_k|^2}{\delta}, \frac{\delta}{\sigma_{24}^2\, \gamma}\right)\right] \underset{0}{\overset{1}{\gtrless}} \eta \tag{16}$$

with η denoting the detector threshold given by

$$\eta \triangleq M \log\left[\frac{\sigma_{24}^2\, \gamma}{\delta} \exp\left(-\frac{\delta}{\sigma_{24}^2\, \gamma}\right)\right] \approx M \log\left\{2\, \mathrm{SIR} \exp[-(2\, \mathrm{SIR})^{-1}]\right\} \tag{17}$$

where the last approximation holds for vanishingly small noise [see eq. (10)]. Therefore, in this scenario, the noncoherent demodulator (16) operates by comparing with a suitable threshold the sum of two contributions: the first one is a scaled version of the squared envelope of

the received signal, whereas the second one is given by $g(\boldsymbol{r}) \triangleq \sum_{k=0}^{M-1} \log\left[K_0\left(\frac{|r_k|^2}{\delta_k}, \frac{\delta_k}{\sigma_{24}^2\,\gamma_{kq}}\right)\right]$, with $\boldsymbol{r} \in \mathcal{H}_C \triangleq [-R_{\max}, R_{\max}]^M$ and $R_{\max} \triangleq \max\{|r_0|, |r_1|, \ldots, |r_{M-1}|\}$.

The rigorous analytical evaluation of the bit-error-rate (BER) for the proposed noncoherent detector represents a very challenging task; for this reason, we will evaluate its performance through numerical simulations reported in Section V. In the next section, instead, we will propose a suboptimal version of the backscatter detector for on-off signaling, whose performance will be evaluated analytically.

IV. SUBOPTIMAL ENERGY DETECTOR FOR ON-OFF-KEYING BACKSCATTER SIGNALING

A suboptimal detector for backscatter communication can be derived by approximating the function $g(\boldsymbol{r}) \triangleq \sum_{k=0}^{M-1} \log\left[K_0\left(\frac{|r_k|^2}{\delta_k}, \frac{\delta_k}{\sigma_{24}^2\,\gamma_{kq}}\right)\right]$ with a *circular* version of it, i.e., $g(\boldsymbol{r}) \approx g_C(\|\boldsymbol{r}\|^2) \triangleq \log\left[K_0\left(\frac{\|\boldsymbol{r}\|^2}{\delta}, \frac{\delta}{\sigma_{24}^2\,\gamma}\right)\right]$, with $\boldsymbol{r}$ no longer belonging to the hypercube $\mathcal{H}_C \triangleq [-R_{\max}, R_{\max}]^M$ with $R_{\max} \triangleq \max\{|r_0|, |r_1|, \ldots, |r_{M-1}|\}$, but to the M-dimensional hypersphere $\mathcal{H}_S \triangleq \{\boldsymbol{r} \in \mathbb{R}^M : \|\boldsymbol{r}\|^2 \leq R_{\max}\}$ of radius $R_{\max}$, inscribed into $\mathcal{H}_C$. In this case, the decision rule (16) can be expressed as

$$\frac{1}{\delta}\,\|\boldsymbol{r}\|^2 + \log\left[K_0\left(\frac{\|\boldsymbol{r}\|^2}{\delta}, \frac{\delta}{\sigma_{24}^2\,\gamma}\right)\right] \underset{0}{\overset{1}{\gtrless}} \eta \tag{18}$$

which shows that the decision is based on the squared envelope of the received signal $\|\boldsymbol{r}\|^2$. Therefore, relying on the monotonicity of the left-hand side of (18) as a function of $\|\boldsymbol{r}\|^2$, detector (18) can be expressed as

$$\|\boldsymbol{r}\|^2 \underset{0}{\overset{1}{\gtrless}} \epsilon \tag{19}$$

with $\epsilon \geq 0$ properly determined, which assumes, thus, the form of the classical energy-detector. Exact computation of ϵ would require numerical inversion of the strongly nonlinear function on the left side of (18); to avoid such a cumbersome task, we alternatively choose ϵ as the threshold which minimizes the error probability of the energy-detector. Its expression is provided by the following lemma:

Lemma 2: The minimum error probability threshold ϵ_{opt} is given by

$$\epsilon_{\text{opt}} = \frac{1}{4}\,\frac{1}{\left(\bar{\lambda}_0^{1/2} - \bar{\lambda}_1^{1/2}\right)^2}\left[\bar{\lambda}_0 - \bar{\lambda}_1 + \sigma_w^2\,(M-1)\,\log\frac{\bar{\lambda}_0}{\bar{\lambda}_1}\right]^2 \tag{20}$$

with

$$\bar{\lambda}_0 \triangleq M\,\sigma_s^2\,\sigma_{14}^2 \tag{21}$$

$$\bar{\lambda}_1 \triangleq M\,\sigma_s^2\,(\alpha^2\,\sigma_{12}^2\,\sigma_{24}^2 + \sigma_{14}^2)\,. \tag{22}$$

Proof: The error probability of the envelope detector (19), conditioned on $\boldsymbol{C}_{12}$, $\boldsymbol{C}_{24}$, $\boldsymbol{C}_{14}$, and $\boldsymbol{s}$, is given by

$$P(e|\boldsymbol{C}_{12}, \boldsymbol{C}_{24}, \boldsymbol{C}_{14}, \boldsymbol{s}) = \frac{1}{2}\int_{\epsilon}^{+\infty} f_{\|\boldsymbol{r}\|^2|\boldsymbol{C}_{14},\boldsymbol{s}}(r;0)\mathrm{d}r + \frac{1}{2}\int_{0}^{\epsilon} f_{\|\boldsymbol{r}\|^2|\boldsymbol{C}_{12},\boldsymbol{C}_{24},\boldsymbol{C}_{14},\boldsymbol{s}}(r;1)\mathrm{d}r \tag{23}$$

where $f_{\|\boldsymbol{r}\|^2|\boldsymbol{C}_{14},\boldsymbol{s}}(r;0)$ ($f_{\|\boldsymbol{r}\|^2|\boldsymbol{C}_{12},\boldsymbol{C}_{24},\boldsymbol{C}_{14},\boldsymbol{s}}(r;1)$) denotes the pdf of the squared envelope $\|\boldsymbol{r}\|^2$, conditioned on $\boldsymbol{C}_{14}$, and $\boldsymbol{s}$ ($\boldsymbol{C}_{12}$, $\boldsymbol{C}_{24}$, $\boldsymbol{C}_{14}$, and $\boldsymbol{s}$), when the transmitted backscatter symbol is equal to $b = 0$ ($b = 1$). From [42], it results that $f_{\|\boldsymbol{r}\|^2|\boldsymbol{C}_{14},\boldsymbol{s}}(r;0)$ and $f_{\|\boldsymbol{r}\|^2|\boldsymbol{C}_{12},\boldsymbol{C}_{24},\boldsymbol{C}_{14},\boldsymbol{s}}(r;1)$ are noncentral chi-square pdfs with $2\,M$ degrees of freedom and noncentral parameters $\lambda_0 \triangleq \sum_{k=1}^{M} |C_{14}(k)|^2\,|s_k|^2$ and $\lambda_1 \triangleq \sum_{k=1}^{M} |\alpha^2\,C_{12}(k)\,C_{24}(k) + C_{14}(k)|^2\,|s_k|^2$, respectively. Therefore, the two integrals in (23) can be expressed in terms of the generalized Marcum's Q function [42], yielding thus

$$P(e|\boldsymbol{C}_{12}, \boldsymbol{C}_{24}, \boldsymbol{C}_{14}, \boldsymbol{s}) = \frac{1}{2}\left[Q_M\left(\sqrt{\frac{\lambda_0}{\sigma_w^2}}, \sqrt{\frac{\epsilon}{\sigma_w^2}}\right) + 1 - Q_M\left(\sqrt{\frac{\lambda_1}{\sigma_w^2}}, \sqrt{\frac{\epsilon}{\sigma_w^2}}\right)\right]. \tag{24}$$

At this point, the error probability $P(e)$ may be computed by statistically averaging, with respect to $\boldsymbol{C}_{12}$, $\boldsymbol{C}_{24}$, $\boldsymbol{C}_{14}$, and $\boldsymbol{s}$, the conditioned error probability $P(e|\boldsymbol{C}_{12}, \boldsymbol{C}_{24}, \boldsymbol{C}_{14}, \boldsymbol{s})$, i.e., $P(e) = \mathbb{E}[P(e|\boldsymbol{C}_{12}, \boldsymbol{C}_{24}, \boldsymbol{C}_{14}, \boldsymbol{s})]$; however, by invoking the strong law of large numbers, we observe that, when the number of subcarriers M is sufficiently large, the noncentral parameters λ_0 and λ_1 converge *almost surely* to their means $\mathbb{E}[\lambda_0] = M\,\sigma_s^2\,\sigma_{14}^2 \triangleq \bar{\lambda}_0$ and $\mathbb{E}[\lambda_1] = M\,\sigma_s^2\,(\alpha^2\,\sigma_{12}^2\,\sigma_{24}^2 + \sigma_{14}^2) \triangleq \bar{\lambda}_1$, respectively, and thus the error probability $P(e)$ of the energy detector can be approximated for $M \gg 1$ as

$$P(e) \approx \frac{1}{2}\left[Q_M\left(\sqrt{\frac{\bar{\lambda}_0}{\sigma_w^2}}, \sqrt{\frac{\epsilon}{\sigma_w^2}}\right) + 1 - Q_M\left(\sqrt{\frac{\bar{\lambda}_1}{\sigma_w^2}}, \sqrt{\frac{\epsilon}{\sigma_w^2}}\right)\right]. \tag{25}$$

By equating to zero the first-order partial derivative of (25), one obtains the following equation

$$\epsilon^{\frac{M-1}{2}}\,e^{-\frac{\epsilon}{2\,\sigma_w^2}}\left\{\frac{e^{-\frac{\bar{\lambda}_0}{2\,\sigma_w^2}}}{\bar{\lambda}_0^{\frac{M-1}{2}}}\,I_{M-1}\left[\frac{(\bar{\lambda}_0\,\epsilon)^{1/2}}{\sigma_w^2}\right] - \frac{e^{-\frac{\bar{\lambda}_1}{2\,\sigma_w^2}}}{\bar{\lambda}_1^{\frac{M-1}{2}}}\,I_{M-1}\left[\frac{(\bar{\lambda}_1\,\epsilon)^{1/2}}{\sigma_w^2}\right]\right\} = 0 \tag{26}$$

where $I_m(a)$ is the modified Bessel function of the first kind [43]. For small σ_w^2 values, we may use the approximation

$I_m(a) \approx e^a$ and rewrite (26) as

$$\exp\left[\frac{\epsilon^{1/2}\left(\bar{\lambda}_0^{1/2}-\bar{\lambda}_1^{1/2}\right)}{\sigma_w^2}\right] = \left(\frac{\bar{\lambda}_0}{\bar{\lambda}_1}\right)^{\frac{M-1}{2}} \exp\left(-\frac{\bar{\lambda}_1-\bar{\lambda}_0}{2\sigma_w^2}\right). \tag{27}$$

Finally, by taking the logarithm of both sides of (27) and solving with respect to ϵ, we obtain (20). ■

By substituting the expressions of $\bar{\lambda}_0$ and $\bar{\lambda}_1$ into (20), it turns out that, as the noise power σ_w^2 approaches zero, the optimal threshold assumes the following approximated expression

$$\epsilon_{\text{opt}} \approx \epsilon_{0,\text{opt}} \frac{\text{SIR}}{1+\text{SIR}-\sqrt{1+2\,\text{SIR}}} \tag{28}$$

with $\epsilon_{0,\text{opt}} \triangleq \frac{1}{4}\,\alpha^2\,M\,\sigma_s^2\,\sigma_{12}^2\,\sigma_{24}^2$, which is a monotonically decreasing function of the SIR. In particular, when the SIR tends to infinity (i.e., when the direct-link interference contribution is negligible), the optimal threshold value tends to $\epsilon_{0,\text{opt}}$, which represents the minimum error probability threshold in the absence of direct-link interference; on the contrary, as the SIR decreases (i.e., the DLI increases), the energies of the received signals under the two hypotheses $b=0$ and $b=1$ tend to increase and, correspondingly, the optimal threshold ϵ_{opt}.

V. NUMERICAL RESULTS

In this section, we provide simulation results aimed at evaluating the performance of the proposed noncoherent detectors.

We assume that the OFDM system, operating at $f_c = 500$ MHz, employs quaternary PSK (QPSK) modulation and consider two different scenarios [44], whose system parameters are listed in Table 1. The considered network topology is depicted in Fig. 1, where the distance between nodes 2 and 4 is set to $\zeta_{24} = (0.5 \cdot \lambda)$, with $\lambda = 0.6$ m denoting the wavelength, when SNR $= 20$ dB, $\gamma = 3/4\pi$, whereas the distance ζ_{12} between nodes 1 and 2 can vary.

The channel taps are modeled as circularly-symmetric complex Gaussian random variables, with path-losses given by [45], [46] $\sigma_{ik}^2 = c^2/(4\pi f_c \zeta_{ik})^2$, for $(i,k) \in \{(1,2),(2,4),(1,4)\}$, where $c = 3{\cdot}10^8$ m/s is the light speed. The channel memories are chosen accordingly to Table 1, whereas the discrete-time propagation delays are fixed to $D_{12} = D_{24} = D_{14} = 0$. We assume that the BD adopts OOK modulation and set $\alpha = 0.6$.

	scenario 1	**scenario 2**
M	512	1024
L_{cp}	40	80
L_{12}	8	12
L_{24}	1	2
L_{14}	3	6

Table 1: Some simulation parameters for the two considered scenarios.

We evaluate the average BER (ABER) through 10^5 Monte Carlo trials, with each run using a different set of symbols, channels and noise samples, and compare the performance of our proposed detectors with that of [21]. In particular, we implement the CP-based energy detector proposed in [21], based on the test statistic $\frac{1}{\sigma_w^2 J}\sum_{L_{\max}}^{L_{\text{cp}}-1}|r(n)|^2$, where $J \triangleq L_{\text{cp}} - L_{\max}$ denotes the unconsumed part of the CP and is equal to $J = 31$ and $J = 66$ for the scenarios 1 and 2, respectively. Moreover, we assume, for the determination of its corresponding threshold, *perfect* knowledge of the composite channel of the link $1 \to 2 \to 4$. It is worth noting that the detector [21] requires the existence of an unconsumed part of the CP, which should be sufficiently long to ensure a suitably high SNR at the reader, and, furthermore, relies on the estimation of the strength of the instantaneous backscatter channel as well as the maximum channel delay spread $L_{\max}$.

In Fig. 2, we focus on the scenario 1 and report the ABER as a function of the ratio ζ_{12}/λ, the distance ζ_{24} between the tag and the reader is fixed to $(0.5 \cdot \lambda)$ and the distance ζ_{14} between the ambient source and the reader is derived through the Carnot's cosine law as $\zeta_{14} = (\zeta_{12}^2 + \zeta_{24}^2 - 2\,\zeta_{12}\,\zeta_{24}\,\cos\gamma)^{1/2}$; from (10), the SIR values corresponding to the distances considered turn out to be equal to -3.05, -3.73, -4.16, -4.45, -4.66 and -4.82 (in dB).

The detectors under comparison are the following:

- the CP-based ED [21];
- the proposed Suboptimal ED employing the threshold (20);
- the proposed Noncoherent ML (16).

From this figure, it is apparent that, in this scenario, both the proposed noncoherent demodulators outperform the CP-based ED; the performance gain tends to monotonically decrease as the tag moves away from the ambient source, i.e., as ζ_{12}/λ increases or, equivalently, SIR decreases. The

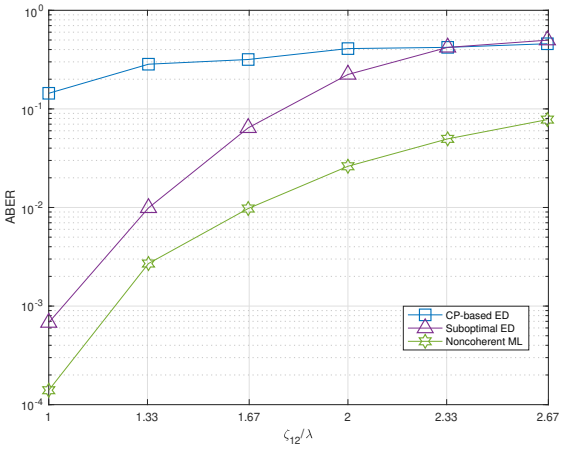

Figure 2: ABER versus ζ_{12}/λ (scenario 1).

Suboptimal ED pays a performance penalty with respect to the Noncoherent ML detector, which is traded-off for a lower complexity burden. Numerical results not reported here show

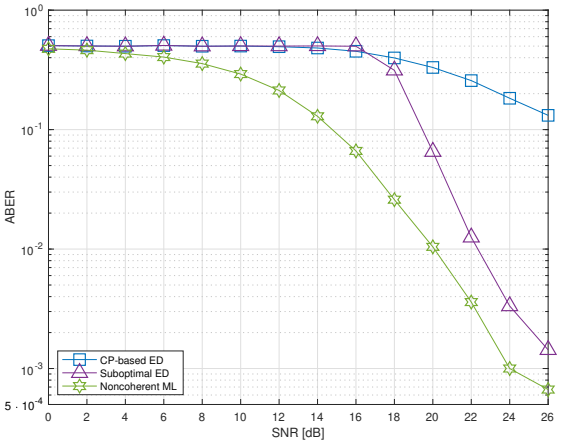

Figure 3: ABER versus SNR (scenario 1).

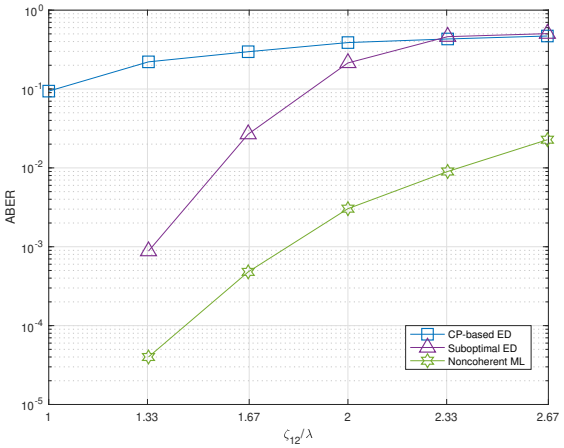

Figure 4: ABER versus ζ_{12}/λ (scenario 2).

that the three detectors under comparison exhibit similar performances when ζ_{12} is kept fixed and, instead, the distance ζ_{24} between the ambient source and the tag varies, as we expected from the theoretical ABER expression (25).

Moreover, we have compared the theoretical ABER curve of our Suboptimal ED, obtained implementing (25), with that obtained via Monte Carlo simulation and the results, not reported here for simplicity, show that both curves perfectly match.

In Fig. 3, we report, for the scenario 1, the ABER curve as a function of the signal-to-noise ratio SNR $\triangleq \sigma_s^2/\sigma_w^2$, when $\zeta_{12} = (1.67 \cdot \lambda)$ and $\zeta_{24} = (0.5 \cdot \lambda)$. Results show that both Noncoherent ML detector and Suboptimal ED perform better than the CP-based ED for all the considered SNR values. The Suboptimal ED, however, exhibits worse performance than the Noncoherent ML detector over the entire range of the SNR; the unsatisfactory performance of the Suboptimal ED, for SNR ranging from 0 to 16 dB, is basically due to the fact that energy-detectors produce high detection error at low SNR [20].

To analyse the dependence of our proposed detectors on the number of subcarriers M, we have reported in Fig. 4 the ABER as a function of ζ_{12}/λ for the scenario 2, characterised by $M = 1024$ and $L_{\text{cp}} = 80$. The CP-based ED, which exploits only the energy of the unconsumed portion of the CP, of length J, performs comparably to the latter scenario; the proposed detectors, instead, which make use of the energy of the entire OFDM block, perform significantly better, especially when the reader is very close to the ambient source.

Finally, in Fig. 5 we have reported the ABER of all the detectors under comparison as a function of the SNR for the scenario 2. The performance results of the two proposed detectors are in good agreement with those obtained for the scenario 1.

It is worth noting that, for both the considered scenarios, when SNR assumes values exceeding 24 dB, the performance of the Noncoherent ML detector and Suboptimal ED exhibit

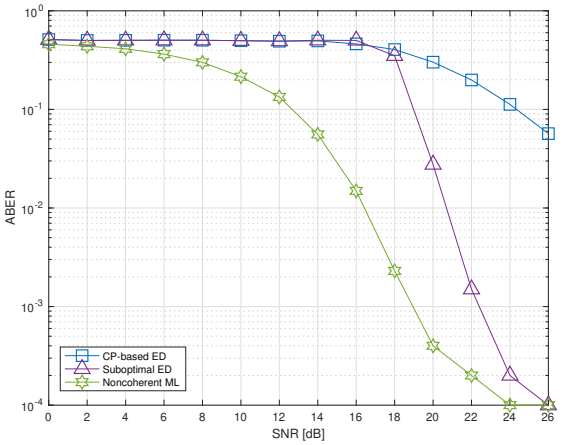

Figure 5: ABER versus SNR (scenario 2).

a BER floor, due to the presence of residual DLI, which cannot be canceled out by increasing SNR. The CP-based ED, instead, does not suffer from this problem, since it uses for backscatter detection a DLI-free portion of the OFDM block.

Finally, we analyse the performance of the proposed Noncoherent ML detector for higher-order modulations; in Figs. 6 and 7, we report the ABER as a function of ζ_{12}/λ and SNR, respectively, for both the scenarios 1 and 2, when the tag uses a ternary constellation. In particular, recalling that, from (13), the backscatter system can employ only non constant-modulus constellations, we assume that the backscatter symbols are independently and equiprobably drawn from the ternary set $B = \{0, 1/2, 1\}$. The system parameters for the two considered scenarios are chosen according to Table 1; the distance between the nodes 2 and 4 is equal to $\zeta_{24} = (0.33 \cdot \lambda)$, whereas we set SNR=24 dB, for Fig. 6, and $\zeta_{12} = (1.67 \cdot \lambda)$, for Fig. 7. As expected, by increasing the constellation size, Noncoherent ML detector

$$f_{\boldsymbol{r}|\boldsymbol{C}_{12},\boldsymbol{C}_{24},\boldsymbol{C}_{14},\boldsymbol{s}}(\boldsymbol{r};\beta_q) = \frac{1}{(\pi\,\sigma_w^2)^M}\,\exp\left\{-\frac{1}{\sigma_w^2}\,\|\boldsymbol{r}-\alpha\,\boldsymbol{C}_{12}\,\boldsymbol{C}_{24}\,\boldsymbol{s}\,\beta_q-\boldsymbol{C}_{14}\,\boldsymbol{s}\|^2\right\}$$

$$= \frac{1}{(\pi\,\sigma_w^2)^M}\prod_{k=0}^{M-1}\exp\left\{-\frac{1}{\sigma_w^2}|r_k-\alpha\,C_{12}(k)\,C_{24}(k)\,s_k\,\beta_q-C_{14}(k)\,s_k|^2\right\}. \quad (30)$$

$$\mathsf{E}_{\boldsymbol{C}_{12}}[f_{\boldsymbol{r}|\boldsymbol{C}_{12},\boldsymbol{C}_{24},\boldsymbol{C}_{14},\boldsymbol{s}}(\boldsymbol{r};\beta_q)] = \frac{1}{(\pi\,\sigma_w^2)^M}\,\mathsf{E}_{\boldsymbol{C}_{12}}\left[\exp\left\{-\frac{1}{\sigma_w^2}\,\|\boldsymbol{r}-\alpha\,\boldsymbol{C}_{12}\,\boldsymbol{C}_{24}\,\boldsymbol{s}\,\beta_q-\boldsymbol{C}_{14}\,\boldsymbol{s}\|^2\right\}\right]$$

$$\frac{1}{(\pi\,\sigma_w^2)^M}\prod_{k=0}^{M-1}\mathsf{E}_{C_{12}(k)}\left[\exp\left\{-\frac{1}{\sigma_w^2}|r_k-\alpha\,C_{12}(k)\,C_{24}(k)\,s_k\,\beta_q-C_{14}(k)\,s_k|^2\right\}\right]. \quad (31)$$

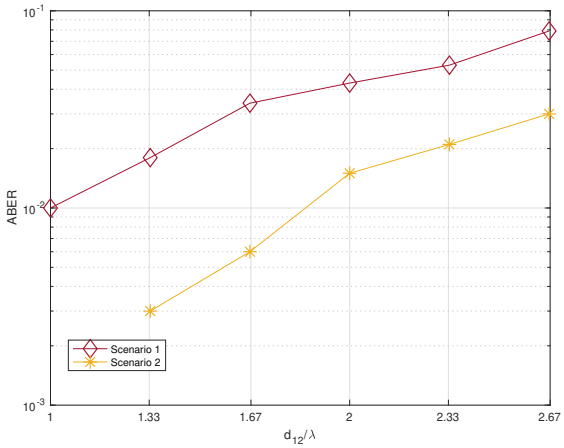

Figure 6: ABER of the Noncoherent ML detector versus d_{12}/λ for scenarios 1 and 2 and ternary constellation.

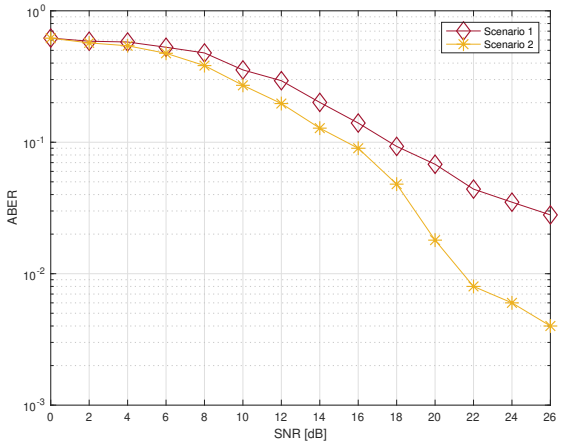

Figure 7: ABER of the Noncoherent ML detector versus SNR for scenarios 1 and 2 and ternary constellation.

exhibits a performance degradation with respect to the OOK case, in both scenarios, which, however, is compensated by an increase of the spectral efficiency.

VI. CONCLUSIONS

This paper dealt with noncoherent detection problem for backscatter communications over ambient OFDM signals. Relying on a minimal set of assumptions, we studied and solved the noncoherent ML detection problem for a general Q-ary signal constellation; in addition, we derived a suboptimal detector, which takes the form of the classical energy-detector (ED), and evaluated its performance in closed-form. Both receivers do not require knowledge or estimation of the instantaneous CSI and ambient OFDM signal. Numerical results showed that our proposed detectors can achieve low bit-error-rate at small distances of the tag from the ambient OFDM source, for moderate SNR values. The achievable bit-error-rate improves as the number of subcarriers increases.

APPENDIX. PROOF OF LEMMA 1

Recalling that $\boldsymbol{w}$ is modeled as a circularly-symmetric complex Gaussian random vector, with covariance matrix $\boldsymbol{K}_{\boldsymbol{w}\boldsymbol{w}} \triangleq \mathsf{E}[\boldsymbol{w}\,\boldsymbol{w}^{\mathrm{H}}] = \sigma_w^2\,\boldsymbol{I}_M$, the multivariate conditional pdf of the received vector $\boldsymbol{r}$, under the q-th hyphotesis, can be expressed [38] as in equation (30) at the top of this page.

Exploiting the statistical independence among the sub-channels $\{C_{12}(k)\}_{k=0}^{M-1}$, the statistical average of (30) with respect to $\boldsymbol{C}_{12}$ reduces to the expression given by (31) at the top of the page. At this point, we observe that, conditioned on $C_{24}(k)$, $C_{14}(k)$ and s_k, the term $\alpha\,C_{12}(k)\,C_{24}(k)\,s_k\,\beta_q + C_{14}\,s_k - r_k \triangleq X_{kq}$ appearing in (31) is distributed as a complex Gaussian random variable, with mean $m_k \triangleq C_{14}(k)\,s_k - r_k$ and variance $\sigma_{kq}^2 \triangleq \alpha^2\,\sigma_{12}^2\,|C_{24}(k)|^2\,|\beta_q|^2\,|s_k|^2$. It can be proven that the pdf of

$|X_{kq}|^2$ is given by

$$f_{|X_{kq}|^2}(x) = \frac{1}{(8\pi x\sigma_{kq}^2)^{1/2}} \left[\exp\left(-\frac{(\sqrt{x}+m_k)^2}{2\,\sigma_{kq}^2}\right) + \exp\left(-\frac{(\sqrt{x}-m_k)^2}{2\,\sigma_{kq}^2}\right)\right] \mathrm{u}(x) \quad (32)$$

and the associated moment-generating function (MGF) $M_{|X_{kq}|^2}(s)$ assumes the following form

$$M_{|X_{kq}|^2}(s) \triangleq \mathsf{E}_{|X_{kq}|^2}[\exp(s\cdot|X_{kq}|^2)] = \frac{\exp\left(\frac{s\,|m_k|^2}{1-2\,s\,\sigma_{kq}^2}\right)}{(1-2\,s\,\sigma_{kq}^2)^{1/2}}\,. \quad (33)$$

On the basis of (33), the statistical average (31) can be, thus, expressed as

$$\mathsf{E}_{\boldsymbol{C}_{12}}[f_{\boldsymbol{r}|\boldsymbol{C}_{12},\boldsymbol{C}_{24},\boldsymbol{C}_{14},\boldsymbol{s}}(\boldsymbol{r};\beta_q)] = \frac{1}{(\pi\,\sigma_w^2)^M}\prod_{k=0}^{M-1} M_{|X_{kq}|^2}\left(-\frac{1}{\sigma_w^2}\right) = \frac{1}{(\pi\,\sigma_w^2)^M} \times \prod_{k=0}^{M-1}\frac{\exp\left(-\frac{1}{\sigma_w^2}\frac{|C_{14}(k)\,s_k-r_k|^2}{1+\frac{1}{\sigma_w^2}\,\alpha^2\,\sigma_{12}^2\,|C_{24}(k)|^2\,|\beta_q|^2\,|s_k|^2}\right)}{1+\frac{1}{\sigma_w^2}\,\alpha^2\,\sigma_{12}^2\,|C_{24}(k)|^2\,|\beta_q|^2\,|s_k|^2}\,. \quad (34)$$

Statistical average with respect to $\boldsymbol{C}_{14}$ is now in order. Let $Y_k \triangleq C_{14}(k)\,s_k - r_k$, it results that, conditioned on s_k, Y_k is Gaussian distributed, with mean $-r_k$ and variance $\sigma_{14}^2\,|s_k|^2$. Hence, invoking again the statistical independence among $\{C_{14}(k)\}_{k=0}^{M-1}$, after some calculations, the average of (34), conditioned on $\boldsymbol{C}_{24}$ and $\boldsymbol{s}$, can be expressed as

$$\mathsf{E}_{\boldsymbol{C}_{14}}[\mathsf{E}_{\boldsymbol{C}_{12}}[f_{\boldsymbol{r}|\boldsymbol{C}_{12},\boldsymbol{C}_{24},\boldsymbol{C}_{14},\boldsymbol{s}}(\boldsymbol{r};\beta_q)]] = \frac{1}{(\pi\sigma_w^2)^M} \times \prod_{k=0}^{M-1}\frac{\mathsf{E}_{C_{14}(k)}\left[\exp\left(-\frac{1}{\sigma_w^2}\frac{|C_{14}(k)s_k-r_k|^2}{1+\frac{1}{\sigma_w^2}\alpha^2\sigma_{12}^2|C_{24}(k)|^2|\beta_q|^2|s_k|^2}\right)\right]}{1+\frac{1}{\sigma_w^2}\alpha^2\sigma_{12}^2|C_{24}(k)|^2|\beta_q|^2|s_k|^2}$$
$$= \frac{1}{(\pi\,\sigma_w^2)^M}\prod_{k=0}^{M-1}\frac{M_{|Y_k|^2}\left(-\frac{1}{\sigma_w^2+\alpha^2\,\sigma_{12}^2\,|C_{24}(k)|^2\,|\beta_q|^2\,|s_k|^2}\right)}{1+\frac{1}{\sigma_w^2}\,\alpha^2\,\sigma_{12}^2\,|C_{24}(k)|^2\,|\beta_q|^2\,|s_k|^2}$$
$$= \frac{1}{(\pi\sigma_w^2)^M}\prod_{k=0}^{M-1}\frac{\sigma_w^2}{\sigma_w^2+\alpha^2\sigma_{12}^2|C_{24}(k)|^2|\beta_q|^2|s_k|^2+\sigma_{14}^2|s_k|^2} \exp\left(-\frac{|r_k|^2}{\sigma_w^2+\alpha^2\,\sigma_{12}^2\,|C_{24}(k)|^2\,|\beta_q|^2\,|s_k|^2+\sigma_{14}^2\,|s_k|^2}\right) \quad (35)$$

where (33) has been taken into account.

Since $C_{24}(k) \sim \mathcal{CN}(0,\sigma_{24}^2)$, its squared value $|C_{24}(k)|^2$, for $k=0,1,\ldots,M-1$, is distributed as an exponential random variable, with parameter $1/\sigma_{24}^2$. Therefore, the statistical average of (35) with respect to $\boldsymbol{C}_{24}$, conditioned on $\boldsymbol{s}$, turns out to be equal to

$$\mathsf{E}_{\boldsymbol{C}_{24}}[\mathsf{E}_{\boldsymbol{C}_{14}}[\mathsf{E}_{\boldsymbol{C}_{12}}[f_{\boldsymbol{r}|\boldsymbol{C}_{12},\boldsymbol{C}_{24},\boldsymbol{C}_{14},\boldsymbol{s}}(\boldsymbol{r};\beta_q)]]] = \frac{\sigma_w^2}{\sigma_{24}^2}\int_0^{+\infty}\frac{1}{\gamma_{kq}\,x+\delta_k}\exp\left(-\frac{|r_k|^2}{\gamma_{kq}\,x+\delta_k}-\frac{x}{\sigma_{24}^2}\right)\mathrm{d}x = \frac{\sigma_w^2}{\sigma_{24}^2\,\gamma_{kq}}\exp\left(\frac{\delta_k}{\sigma_{24}^2\,\gamma_{kq}}\right)K_0\left(\frac{|r_k|^2}{\delta_k},\frac{\delta_k}{\sigma_{24}^2\,\gamma_{kq}}\right) \quad (36)$$

where we let $\gamma_{kq} \triangleq \alpha^2\,\sigma_{12}^2\,|\beta_q|^2\,|s_k|^2 \neq 0$, $\delta_k \triangleq \sigma_w^2 + \sigma_{14}^2\,|s_k|^2$, and

$$K_0(x,y) = \int_1^{+\infty} t^{-1}\,\mathrm{e}^{-x\,t-y\,t^{-1}}\,\mathrm{d}t$$

is the *leaky aquifer function* [39].

When $\gamma_{kq}=0$, e.g., if the backscatter and/or legacy constellation contains the information symbol zero, the statistical average of (35) with respect to $\boldsymbol{C}_{24}$, conditioned on $\boldsymbol{s}$, is evaluated as

$$\mathsf{E}_{\boldsymbol{C}_{24}}[\mathsf{E}_{\boldsymbol{C}_{14}}[\mathsf{E}_{\boldsymbol{C}_{12}}[f_{\boldsymbol{r}|\boldsymbol{C}_{12},\boldsymbol{C}_{24},\boldsymbol{C}_{14},\boldsymbol{s}}(\boldsymbol{r};\beta_q)]]] = \frac{\sigma_w^2}{\sigma_{24}^2\,\delta_k}\exp\left(-\frac{|r_k|^2}{\delta_k}\right)\int_0^{+\infty}\exp\left(-\frac{x}{\sigma_{24}^2}\right)\mathrm{d}x = \frac{\sigma_w^2}{\delta_k}\exp\left(-\frac{|r_k|^2}{\delta_k}\right)\,. \quad (37)$$

The decision rule (13) is finally obtained by averaging (36) or (37) with respect to the statistical distribution of the OFDM legacy symbol $\boldsymbol{s}$.

References

[1] L. Tan and N. Wang, "Future Internet: The Internet of Things," Proc. IEEE ICACTE, pp. V5-376–V5-380, August 2010.

[2] "Towards a Definition of the Internet of Things (IoT)," Available online: https://iot.ieee.org/images/files/pdf/IEEE_IoT_Towards_Definition_Internet_of_Things_Revision1_27MAY15.pdf.

[3] A. Ghasempour, "Internet of Things in Smart Grid: Architecture, Applications, Services, Key Technologies, and Challenges," Inventions, March 2019.

[4] G. Vannucci, A. Bletsas, and D. Leigh, "A software-defined radio system for backscatter sensor networks," IEEE Trans. Wireless Commun., vol. 7, pp. 2170–2179, June 2008.

[5] J. Kimionis, A. Bletsas, and J. N. Sahalos, "Increased range bistatic scatter radio," IEEE Trans. Wireless Commun., vol. 62, pp. 1091–1104, Mar. 2014.

[6] E. Kampianakis, J. Kimionis, K. Tountas, C. Konstantopoulos, E. Koutroulis, and A. Bletsas, "Wireless environmental sensor networking with analog scatter radio & timer principles," IEEE Sensors J., vol. 14, pp. 3365–3376, Oct. 2014.

[7] N. Fasarakis-Hilliard,P. N. Alevizos, and A. Bletsas, "Coherent detection and channel coding for bistatic scatter radio sensor networking," IEEE Trans. Commun., vol. 63, pp. 1798–1810, May 2015.

[8] P. N. Alevizos, A. Bletsas, and G. N. Karystinos, "Noncoherent short packet detection and decoding for scatter radio sensor networking," IEEE Trans. Commun., vol. 65, pp. 2128–2140, May 2017.

[9] V. Chawla and D. S. Ha, "An overview of passive RFID," IEEE Commun. Mag., vol. 45, pp. 11–17, Sep. 2007.

[10] C. Boyer and S. Roy, "Backscatter communication and RFID: Coding, energy, and MIMO analysis", IEEE Trans. Wireless Commun., vol. 62, pp. 770–785, March 2014.

[11] V. Liu, A. Parks, V. Talla, S. Gollakota, D. Wetherall, and J. R. Smith "Ambient backscatter: Wireless communication out of thin air", Proc. of ACM SIGCOMM'13, pp. 39–50, 2005.

[12] N. Van Huynh, D. T. Hoang, X. Lu, D. Niyato, P. Wang, and D. I. Kim "Ambient backscatter communications: a contemporary survey", IEEE Communications surveys & tutorials, vol. 20, no. 4, pp. 2889–2922, fourth quarter 2018.
[13] B. Lyu, C. You, Z. Yang, and G. Gui, "The optimal control policy for RF-powered backscatter communication networks," IEEE Trans. Veh. Technol., vol. 67, pp. 2804–2808, Mar. 2018.
[14] Z. Mat, T. Zeng, G. Wang, and F. Gao, "Signal detection for ambient backscatter system with multiple receiving antennas," IEEE 14th Canadian Workshop Inf. Theory, Jul. 2015, pp. 50–53.
[15] W. S. Lee, C. H. Kang, Y. K. Moon, and H. K. Song, "Determination scheme for detection thresholds using multiple antennas in Wi-Fi backscatter systems," IEEE Access, vol. 5, pp. 22159–22165, 2017.
[16] R. Duan, R. Jantti, M. A. ElMossallamy, Z. Han, and M. Pan, "Multi-antenna receiver for ambient backscatter communication systems," Proc. IEEE Workshop on Signal Process. Advances in Wireless Commun. (SPAWC), Kalamata, Greece, Jun. 2018, pp. 1–5.
[17] C. Chen, G. Wang, L. Fan, F. Verde, and H. Guan, "Detection of ambient backscatter signals from multiple-antenna tags," Proc. IEEE Workshop on Signal Process. Advances in Wireless Commun. (SPAWC), Kalamata, Greece, Jun. 2018, pp. 1–5.
[18] A. Parks, A. Liu, S. Gollakota, and J. R. Smith, "Turbocharging Ambient Backscatter Communication," Proc. ACM SIGCOMM 2014, pp. 619–630, Aug. 2014, Chicago, USA.
[19] C. H. Kang, W. S. Lee, Y. H. You, and H. K. Song, "Signal detection scheme in ambient backscatter system with multiple antennas," IEEE Access, vol. 5, pp. 14543–14547, 2017.
[20] T. Zeng, G. Wang, Y. Wang, Z. Zhong, and C. Tellambura, "Statistical covariance based signal detection for ambient backscatter communication systems," IEEE 84th Vehicular Technology Conference (VTC-Fall), Sept. 2016, pp. 1–5.
[21] G. Yang, Y-C. Liang, R. Zhang, and Y. Pei, "Modulation in the air: backscatter communication over ambient OFDM carrier," IEEE Trans. Commun., vol. 66, pp. 1219–1233, March 2018.
[22] M. A. ElMossallamy, M. Pan, R. Jantti, K. G. Seddik, G. Y Li and Z. Han, "Noncoherent Backscatter Communications over Ambient OFDM Signals," IEEE Trans. Commun., 2019.
[23] D. Darsena, G. Gelli, and F. Verde, "Cloud-aided cognitive ambient backscatter wireless sensor networks," IEEE Access, vol. 7, pp. 57399–57414, May 2019.
[24] J. Qian, F. Gao, G. Wang, S. Jin, and H. Zhu, "Semi-Coherent detection and performance analysis for ambient backscatter system," IEEE Trans. Wireless Commun., vol. 65, pp. 5266–5279, January 2017.
[25] Y. Liu, G. Wang, Z. Dou, and Z. Zhong, "Coding and detection schemes for ambient backscatter communication systems," IEEE Access, vol. 5, pp. 4947–4953, April 2017.
[26] Q. Tao, C. Zhong, H. Lin, and Z. Zhang, "Symbol Detection of Ambient Backscatter Systems with Manchester Coding," IEEE Trans. Wireless Commun., vol. 17, pp. 4028–4038, June 2018.
[27] J. Qian, F. Gao, G. Wang, S. Jin, and H. Zhu, "Noncoherent Detections for Ambient Backscatter System," IEEE Trans. Wireless Commun., vol. 16, pp. 1412–1422, March 2017.
[28] G. Wang, F. Gao, R. Fan, and C. Tellambura, "Ambient Backscatter Communication Systems: Detection and Performance Analysis," IEEE Trans. Commun., vol. 64, pp. 4836–4846, Nov. 2016.
[29] P. Liu, C.. Nie, T. Korakis, E. Erkip, S. S. Panwar, F. Verde, and A. Scaglione "STiCMAC: A MAC Protocol for Robust Space-Time Coding in Cooperative Wireless LANs", IEEE Trans. Wireless Commun., vol. 11, pp. 1358–1369, April 2012.
[30] F. Verde, T. Korakis, E. Erkip, and A. Scaglione "A Simple Recruitment Scheme of Multiple Nodes for Cooperative MAC", IEEE Trans. Commun., vol. 58, pp. 2667–2682, Sep. 2010.

[31] M. Morelli, C. -. J. Kuo and M. Pun, "Synchronization Techniques for Orthogonal Frequency Division Multiple Access (OFDMA): A Tutorial Review," in Proceedings of the IEEE, vol. 95, pp. 1394–1427, July 2007.
[32] P. N. Alevizos and A. Blestas, "Sensitive and nonlinear far-field RF energy harvesting in wireless communications," IEEE Trans. Wireless Commun., vol. 17, pp. 3670–3685, June 2018.
[33] A.V. Oppenheim and R. W. Schafer, Discrete-Time Signal Processing, 3rd Edition, Prentice Hall, Upper Saddle River.
[34] R. Savoia and F. Verde, "Performance Analysis of Distributed Space-Time Block Coding Schemes in Middleton Class-A Noise", IEEE Trans. Veh. Technol., vol. 62, pp. 2579–2595, Jan. 2013.
[35] D. Darsena, G. Gelli, and F. Verde, "Modeling and performance analysis of wireless networks with ambient backscatter devices", IEEE Trans. Commun., vol. 65, Apr. 2017.
[36] D. Tse and P. Viswanath, Fundamentals of wireless communication, Cambridge University Press, 2005.
[37] H. L. Van Trees, Detection, estimation, and modulation theory: detection, estimation, and linear modulation theory, John Wiley and Sons, Inc., 2001.
[38] A. Papoulis. Probability, Random variables, and Stochastics Processes (3rd ed.)., McGraw-Hill, Singapore, 1991.
[39] N. M. Temme, "The leaky aquifer function revisited", International Journal of Quantum Chemistry, vol. 109, pp. 2826–2830, 2009.
[40] S. Benedetto and E. Biglieri, Principles of digital transmission: with wireless applications. Plenum Pub Corp, 1999.
[41] F. E. Harris, "Incomplete Bessel, generalized incomplete gamma, or leaky aquifer functions", Journal of Computational and Applied Mathematics, vol. 215, pp. 260–269, 2008.
[42] J.G. Proakis, Digital Communications, 4th Edition, McGraw-Hill, 2001.
[43] M. Abramowitz and I. Stegun, Handbook of Mathematical Functions with Formulas, Graphs, and Mathematical Tables, Dover, New York, 1964.
[44] A. Ghosh, J. Zhang, J. G. Andrews, and R. Muhamed, Fundamentals of LTE, 1st ed. Upper Saddle River, NJ, USA: Prentice-Hall, 2010.

[45] J. D. Griffin and G. D. Durgin, "Complete link budgets for backscatter-radio and RFID systems," IEEE Antennas and Propagation Magazine vol. 51, pp. 11–25, April 2009.

[46] M. U. Sheikh, R. Duan, and R. Jantti, "Validation of Backscatter Link Budget Simulations with Measurements at 915 MHz and 2.4 GHz," IEEE 89th Vehicular Technology Conference (VTC2019-Spring), Kuala Lumpur, Malaysia, May 2019.